Estimation of ATMS Antenna Emission From Cold Space Observations

Hu Yang, *Member, IEEE*, Fuzhong Weng, and Kent Anderson

***Abstract*—The Advanced Technology Microwave Sounder (ATMS) on board the Suomi National Polar-orbiting Partnership (NPP) satellite is a total power radiometer and scans across the track with a range of $\pm 52.77^\circ$ from nadir. It has 22 channels and measures the microwave radiation at either quasi-vertical or quasi-horizontal polarization from the Earth's atmosphere. The ATMS scanning reflector is made of beryllium coated with gold and can have an emission due to the surface roughness. During prelaunch phase, an estimate of the reflector emissivity was not explored. In this paper, a new methodology is developed to assess the antenna emission from the ATMS pitch-over observations. It is found that the antenna emission is significant and dominates the scan-angle-dependent features in the ATMS antenna temperatures. Retrieved emissivity from K- to G-bands ranges from 0.002 to 0.006. An error model was also developed to assess the impact of antenna emissivity to calibration accuracy of antenna temperature products. Simulation results show that the calibration error is scene temperature dependent and can be as large as 2.5 K for space view.**

***Index Terms*—Advanced technology microwave sounder (ATMS), antenna emissivity, Suomi National Polar-orbiting Partnership (SNPP).**

I. Introduction

ON OCTOBER 28, 2011, the Suomi National Polar-orbiting Partnership (SNPP) satellite was successfully launched into a circular near-polar afternoon-configured (1:30 P.M.) orbit at an average altitude of 842 km above the Earth and an inclination angle of 98.7° to the Equator. The Advanced Technology Microwave Sounder (ATMS) onboard the SNPP satellite profiles atmospheric temperature and moisture in all-weather conditions and supports continuing advances in numerical weather prediction (NWP) for improved short- to medium-range weather forecast skills [1]. The ATMS instrument characteristics are listed in Table I. On February 20, 2012, the ATMS on the SNPP satellite was commanded to pitch over, scan the deep space, and collect 18-min of data with 96 fields of view along each scan. In principle, the brightness temperatures after calibration from the cold space should be uniform across the scan. In our previous studies, it has been found that the pitch maneuver data showed a scan-angle-dependent radiometric bias with respect to the cold space background brightness temperature of 2.73 K. In particular, the biases at ATMS channels 1, 2, and 16 are a sine-squared function of the scan angle (smile shape), whereas the rest of the channels are a cosine-squared function of the scan angle (frown shape) [2]. We also demonstrated that the near-field radiation from the satellite platform and the instrument itself may contribute to the observed scan-angle-dependent bias. An empirical model is then established to explain the scan-angle-dependent feature of ATMS measurement bias, with model parameters derived from the pitch-over maneuver data. The quasi-vertical (QV) and quasi-horizontal (QH) polarized corrections are expressed as a function of the scan angle, i.e.,

$$S_a^{\mathrm{Qv}} = \beta_0 + \beta_1 \sin^2\theta \tag{1a}$$

$$S_a^{\mathrm{QH}} = \beta_0 + \beta_1 \cos^2\theta \tag{1b}$$

where θ is the scan angle, and β_0 and β_1 are the model parameters determined from the pitch maneuver data. The scan-angle-dependent features of antenna brightness temperature for both QV and QH polarizations simulated from the antenna gain data are consistent with maneuver measurements. At nadir, the observed and simulated antenna brightness temperatures have a minimum at all QV channels and a maximum at all QH channels.

Scan-angle-dependent biases are common to microwave sounding instruments. Saunders *et al.* found that scan-angle-dependent bias existed in the AMSU-B instrument during the thermal-vacuum test. They found that the bias is polarization dependent and is larger in nadir than in scan edge [3]. An explanation of this bias, in terms of scan mirror reflectivity, has been given in [4]. By studying the pitch-over observations from the NOAA-14 MSU instrument, Kleespies *et al.* also found that there is a marked asymmetry in the nominal Earth scene, and the characteristics of the asymmetry differ for the different polarizations. The vertically polarized channels display maximum difference from the space look near the nominal nadir position, whereas the horizontally polarized channels tend to have a maximum in the lower scan positions and a minimum in the higher scan positions [5]. In a follow-on study, Kleespies pointed out that the possible root cause of the scan-angle-dependent bias observed in pitch-over observations is the contamination from the Earth sidelobe and the thermal emission from the polarized scan mirror [6].

Study on the F16-SSMIS instrument shows that thermal radiation from the antenna reflector can be a major cause

Manuscript received June 5, 2015; revised November 3, 2015, February 16, 2016, and March 10, 2016; accepted March 11, 2016. Date of publication April 20, 2016; date of current version June 1, 2016.

H. Yang is with University of Maryland, College Park, MD 20742 USA (e-mail: hu.yang@noaa.gov).

F. Weng is with NOAA Center for Satellite Applications and Research, College Park, MD 20740 USA.

K. Anderson is with Northrop Grumman Electronic Systems, Linthicum Heights, MD 21090 USA.

Color versions of one or more of the figures in this paper are available online at http://ieeexplore.ieee.org.

Digital Object Identifier 10.1109/TGRS.2016.2542526

0196-2892 © 2016 IEEE. Translations and content mining are permitted for academic research only. Personal use is also permitted, but republication/redistribution requires IEEE permission. See http://www.ieee.org/publications_standards/publications/rights/index.html for more information.

TABLE I
SNPP ATMS CHANNEL CHARACTERISTICS (K-BAND FOR CHANNELS 1 AND 2, V-BAND FOR CHANNELS 3–15, W-BAND FOR CHANNEL 16, AND G-BAND FOR CHANNELS 17–22)

Ch	Channel Central Freq. (MHz)	Polarization	Bandwidth Max. (MHz)	Frequency Stability (MHz)	Calibration Accuracy (K)	NEΔT (K)	3-dB Bandwidth (deg)
1	23800	QV	270	10	1.0	0.5	5.2
2	31400	QV	180	10	1.0	0.6	5.2
3	50300	QH	180	10	0.75	0.7	2.2
4	51760	QH	400	5	0.75	0.5	2.2
5	52800	QH	400	5	0.75	0.5	2.2
6	53596±115	QH	170	5	0.75	0.5	2.2
7	54400	QH	400	5	0.75	0.5	2.2
8	54940	QH	400	10	0.75	0.5	2.2
9	55500	QH	330	10	0.75	0.5	2.2
10	57290.344(f_o)	QH	330	0.5	0.75	0.75	2.2
11	f_o± 217	QH	78	0.5	0.75	1.0	2.2
12	f_o±322.2±48	QH	36	1.2	0.75	1.0	2.2
13	f_o±322.2±22	QH	16	1.6	0.75	1.5	2.2
14	f_o±322.2±10	QH	8	0.5	0.75	2.2	2.2
15	f_o±322.2±4.5	QH	3	0.5	0.75	3.6	2.2
16	88200	QV	2000	200	1.0	0.3	2.2
17	165500	QH	3000	200	1.0	0.6	1.1
18	183310±7000	QH	2000	30	1.0	0.8	1.1
19	183310±4500	QH	2000	30	1.0	0.8	1.1
20	183310±3000	QH	1000	30	1.0	0.8	1.1
21	183310±1800	QH	1000	30	1.0	0.8	1.1
22	183310±1000	QH	500	30	1.0	0.9	1.1

of calibration bias [7], [8]. For the spaceborne microwave sounding instruments, the antenna reflector is required to be designed with a reflectivity of larger than 0.999. However, the study on special sensor microwave imager/sounder calibration shows that the SIOx coating on the reflector surface may result in reduced reflectivity and, consequently, significant emission [9]. The reflection coefficient for a specimen of the reflector material can be measured with a network analyzer. However, if the reflection coefficient is close to one, it becomes difficult, if not impossible, to achieve the measurement accuracy from the analyzer [10].

The root cause of the scan-angle-dependent bias observed in microwave sounding instrument temperature data record (TDR) products has not been widely discussed in the open literature. In this paper, based on the study from different researchers on legacy NOAA MSU and AMSU instruments, as well as the analysis for on-orbit pitch-over observations from the newest SNPP ATMS instrument, a theoretical model was established to explain the major root cause of the scan-angle-dependent bias observed in NOAA microwave sounding instruments. This model is built based on the assumption that the polarization dependence of the scan mirror reflectivity plays a major role for the observed bias. A retrieval algorithm is then developed to get antenna reflector emissivity from ATMS cold space scan measurements during NPP satellite pitch-over operation. In Section II, a general reflector emission model is introduced. Section III is devoted for the model applied for pitch-over observations; the emissivity retrieval model and its impacts to calibration accuracy are described in Section IV. The summary and discussion on the retrieval products and their possible applications is presented in Section V.

II. ANTENNA REFLECTION AND EMISSION MODEL

A. Characteristics of the ATMS Antenna Reflector

ATMS has two receiving antennas, with one receiving antenna serving for channels 1–15 with frequencies below 60 GHz and a separate receiving antenna for channels 16–22 with frequencies above 60 GHz. As shown in Fig. 1(a), the antennas consist of a plane reflector mounted on a scan axis at a 45° tilt angle so that radiation is reflected from a direction perpendicular to the scan axis into a direction along the scan axis (i.e., a 90° reflection). With the scan axis oriented in the along-track direction, this results in a cross-track scan pattern. The reflected

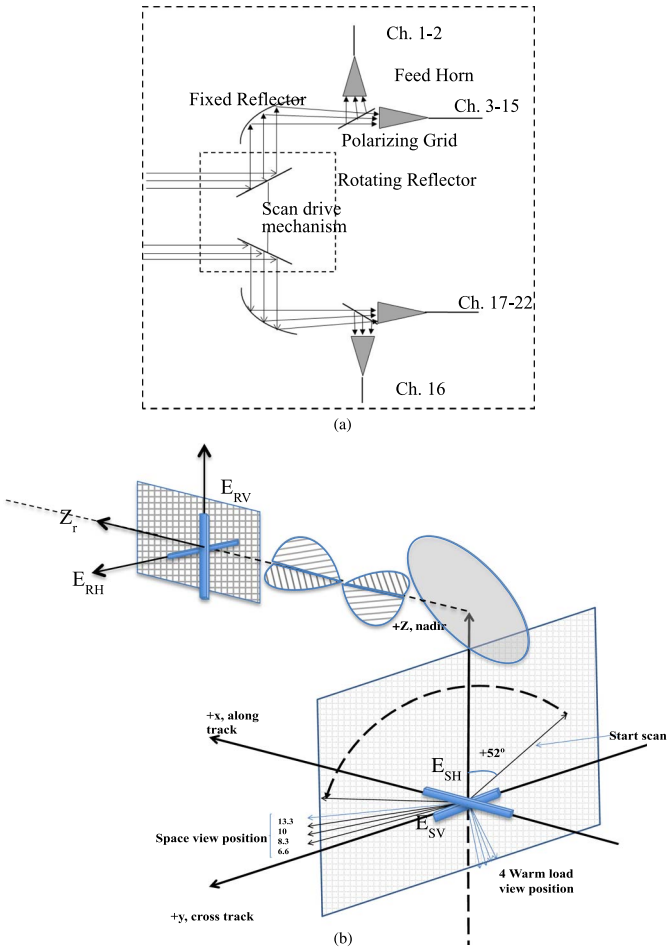

Fig. 1. (a) Schematic of the ATMS antenna subsystem. The top portion shows the antenna subsystem for K-/Ka- and V-bands, whereas the lower portion is for W-/G-bands. (b) Sketch plot for polarization direction definition by taking the scan plane and the reflection plane as reference frames, respectively.

radiation is focused by a stationary parabolic reflector onto a dichroic plate (polarizing grid) and then either reflected to or passed through to a feedhorn. Each aperture/reflector serves two frequency bands, for a total of four bands.

Due to the coating material used, the rotating plane reflector is not lossless and has its own thermal emission. According to Niels Skou's equation [10], the emissivity of a good conducting surface, viewed at normal incidence, is

$$\varepsilon_N = \frac{1}{15}\sqrt{\frac{f}{\sigma \cdot 10^7}}$$

where f is the receiver microwave frequency, and σ is the conductivity of the reflecting surface. This equation should be valid for perfectly smooth and pure bulk conductive materials. For example, for bulk gold ($\sigma = 4.10E7$), the equation gives 0.0014 at 183 GHz and 0.0005 at 23.8 GHz. The actual emissivity of real reflector surfaces is invariably greater than the computed theoretical value, due primarily to surface roughness and impurities. The ATMS flight reflector is made of beryllium with a nominally 0.6-μm gold plating layer, on a nickel interfacing layer. Since the gold plating thickness is comparable with the skin depth, and is likely to have extreme microscopic granularity and roughness, it is not unexpected that the emissivity would greatly exceed the values computed from Skou's equation.

B. Mueller Matrices for Antenna Reflection and Transmission at 45° Incident Angle

As aforementioned, the rotating flat reflector of ATMS has a polarization-dependent reflectivity. To evaluate its impact on reflected radiation, a full polarized physical model for antenna reflection needs to be established first. Fig. 1(b) shows how the scene radiation is reflected by the scan mirror. $E_{\rm sv}$ and $E_{\rm sh}$ are the vertical and horizontal polarization electronic vectors in the scene incident plane, by which the instrument polarization is defined as E-field perpendicular to the plane for H-pol and parallel to the plane for V-pol. $E_{\rm Rv}$ and $E_{\rm Rh}$ are the V- and H-pol electronic vectors in the reflector scan plane, by which the reflection polarization is defined as E-field perpendicular to the plane for H-pol and parallel to the plane for V-pol. Taking the reflector scan plane as a reference, for a homogeneous bulk-material reflector, the Mueller matrices for reflection, i.e., M_R, and emission, i.e., M_T, at an incidence angle of 45° can be expressed as (2a) and (2b) [11], shown at the top of the next page, where θ_r is the refractive angle which is related to the incident angle through Snell's law, and the value of θ_r is close to zero for a metal.

When the ATMS antenna reflector scans to cold space or a blackbody target, the incident radiation is unpolarized and can be expressed in a Stokes vector as

$$S = I_0 \begin{bmatrix} 1 \\ 0 \\ 0 \\ 0 \end{bmatrix} \tag{3}$$

where I_0 is the radiance intensity. From (2a) and (2b), the reflected and emitted Stokes components can be derived by multiplying (3) as

$$S_R = I_0 \frac{1-\sin 2\theta_r}{(1+\sin 2\theta_r)^2} \begin{bmatrix} 1 \\ \sin 2\theta_r \\ 0 \\ 0 \end{bmatrix} \tag{4a}$$

$$S_T = I_0 \frac{2\sin 2\theta_r}{(1+\sin 2\theta_r)^2} \begin{bmatrix} \frac{1}{2}(1+\sin 2\theta_r)+1 \\ \frac{1}{2}(1+\sin 2\theta_r)-1 \\ 0 \\ 0 \end{bmatrix}. \tag{4b}$$

Here, subscripts R and T stand for reflection and emission of incident wave, respectively. Note that the sum of the reflected intensity and the emitted intensity is equal to the incident intensity, i.e.,

$$S = S_R + S_T$$

which is required from the principle of the conservation of energy. It is also interesting to note that, after reflection, the incident unpolarized wave can become polarized, depending on the angle. It should be noted that, in this context, polarization direction is defined in the Earth surface scattering plane instead of in the reflector scanning plane: vertical polarization means

$$M_R = \frac{1-\sin 2\theta_r}{(1+\sin 2\theta_r)^2}\begin{bmatrix} 1 & \sin 2\theta_r & 0 & 0 \\ \sin 2\theta_r & 1 & 0 & 0 \\ 0 & 0 & -\cos 2\theta_r & 0 \\ 0 & 0 & 0 & -\cos 2\theta_r \end{bmatrix} \tag{2a}$$

$$M_T = \frac{2\sin 2\theta_r}{(1+\sin 2\theta_r)^2}\begin{bmatrix} \frac{1+\sin 2\theta_r}{2}+1 & \frac{1+\sin 2\theta_r}{2}-1 & 0 & 0 \\ \frac{1+\sin 2\theta_r}{2}-1 & \frac{1+\sin 2\theta_r}{2}+1 & 0 & 0 \\ 0 & 0 & \sqrt{2}(\cos\theta_r+\sin\theta_r) & 0 \\ 0 & 0 & 0 & \sqrt{2}(\cos\theta_r+\sin\theta_r) \end{bmatrix} \tag{2b}$$

E-field parallel to the scattering plane, and horizontal polarization means $E-$field perpendicular to the scattering plane. For a reflection problem we are studying, it is more convenient to convert the reflected and emitted vectors in (4a) and (4b) to modified Stokes vectors as follows:

$$S_R = \begin{bmatrix} S_{\mathrm{RV}} \\ S_{\mathrm{RH}} \\ S_{R3} \\ S_{R4} \end{bmatrix} = \frac{I_0}{2}\frac{1-\sin 2\theta_r}{(1+\sin 2\theta_r)^2}\begin{bmatrix} 1-\sin 2\theta_r \\ 1+\sin 2\theta_r \\ 0 \\ 0 \end{bmatrix} \tag{5a}$$

$$S_T = \begin{bmatrix} S_{TV} \\ S_{TH} \\ S_{T3} \\ S_{T4} \end{bmatrix} = \frac{I_0}{2}\frac{2\sin 2\theta_r}{(1+\sin 2\theta_r)^2}\begin{bmatrix} 2 \\ 1+\sin 2\theta_r \\ 0 \\ 0 \end{bmatrix}. \tag{5b}$$

From (5a) and (5b), the horizontal and vertical amplitude reflection coefficients of the antenna reflector can be expressed as

$$r_h = \frac{1-\sin 2\theta_r}{1+\sin 2\theta_r} \qquad r_v = \frac{(1-\sin 2\theta_r)^2}{(1+\sin 2\theta_r)^2}. \tag{6a}$$

Similarly, we can obtain the emission coefficients

$$t_h = \frac{2\sin 2\theta_r}{(1+\sin 2\theta_r)} \qquad t_v = \frac{4\sin 2\theta_r}{(1+\sin 2\theta_r)^2}. \tag{6b}$$

From (6a) and (6b), we can see that

$$r_h + t_h = 1 \qquad r_v + t_v = 1.$$

A corresponding relation exists between polarization reflection coefficients, i.e.,

$$r_h^2 = r_v. \tag{7}$$

Note that the preceding relationship is true only at an incident angle of 45°. Later, we will show that the relationship expressed in (7) will be very useful for determination of antenna emissivity or reflectivity.

III. ATMS Antenna Reflection Model for Pitch-Over Observations

As described in the previous section, it is very difficult to measure the ATMS antenna reflectivity from the ground tests. Here, we prove that ATMS pitch-over observations can be used to quantify the antenna loss. When the reflector scans to an angle of θ relative to the feedhorn orientation, the received antenna brightness temperature is a combination of the vertical and horizontal components [2]. Thus, the resulting signals reflected off the antenna can be expressed in the Stokes vector [12], i.e.,

$$R_Q = \begin{bmatrix} R_{\mathrm{Qv}} \\ R_{\mathrm{Qh}} \\ R_{Q3} \\ R_{Q4} \end{bmatrix} = \begin{bmatrix} \cos^2\theta & \sin^2\theta & \frac{1}{2}\sin 2\theta & 0 \\ \sin^2\theta & \cos^2\theta & -\frac{1}{2}\sin 2\theta & 0 \\ -\sin 2\theta & \sin 2\theta & \cos 2\theta & 0 \\ 0 & 0 & 0 & 1 \end{bmatrix} \times (S_R + S_T). \tag{8}$$

where S_R is the cold space radiation reflected by the antenna reflector, and S_T is the thermal radiation from the reflector. Their polarization state is defined in the incident plane (scan plane). As discussed in Section II, S_R and S_T can be expressed as a function of the reflectivity of the scan reflector by substituting (6) into (5), i.e.,

$$S_R = R_S\frac{1-\sin 2\theta_r}{(1+\sin 2\theta_r)^2}\begin{bmatrix} 1+\sin 2\theta_r \\ 1-\sin 2\theta_r \\ 0 \\ 0 \end{bmatrix} = \begin{bmatrix} r_h R_S \\ r_h^2 R_S \\ 0 \\ 0 \end{bmatrix} \tag{9a}$$

$$S_T = R_{\mathrm{rfl}}\frac{2\sin 2\theta_r}{(1+\sin 2\theta_r)^2}\begin{bmatrix} 1+\sin 2\theta_r \\ 2 \\ 0 \\ 0 \end{bmatrix} = \begin{bmatrix} (1-r_h)R_{\mathrm{rfl}} \\ \left(1-r_h^2\right)R_{\mathrm{rfl}} \\ 0 \\ 0 \end{bmatrix}. \tag{9b}$$

In (9), R_s is the scene radiance, and R_{rfl} is the thermal radiance from the antenna reflector itself. It needs be noted that, to derive (8) and (9), the reference incident plane by which the polarization direction is defined is different. As shown in Fig. 1(b), for ATMS observations, the incident plane is formed by the beam direction and the normal direction of the local plane in Earth surface ($E_{\mathrm{SV}} - \mathrm{Z}$ plane in the figure). On the other hand, for the radiation reached in front of the antenna reflector, the incident plane is formed by the beam direction and the normal direction of the antenna plane (Erv$-$Zr plane in the figure). Since the two planes are perpendicular to each other, the V and H directions in these two planes are opposite.

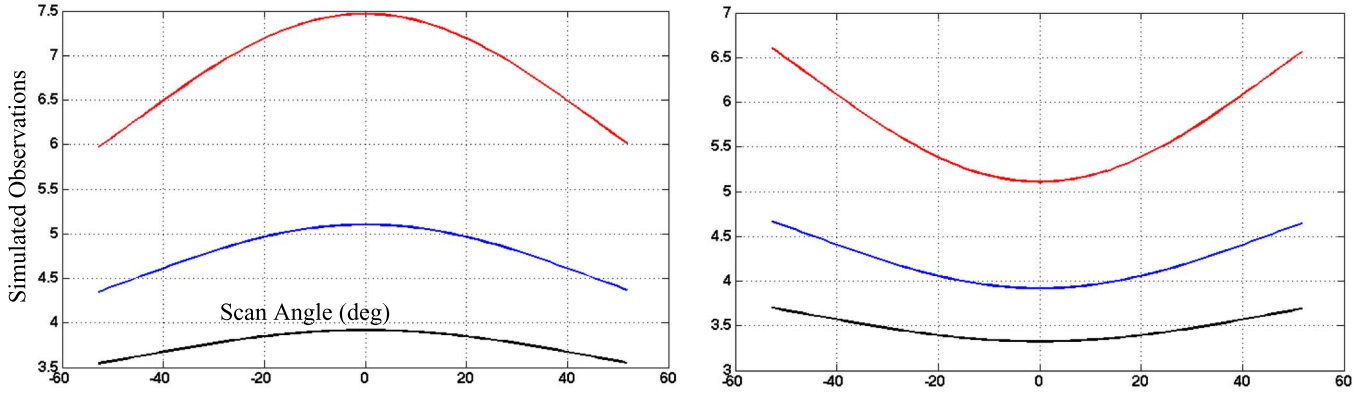

Fig. 2. Simulated cold space observations for (left) QH and (right) QV channels. The scene temperature is set to 2.73 K; the reflector physical temperature is set to 300 K. The red, blue, and black lines correspond to antenna reflectivities of 0.992, 0.996, and 0.998, respectively.

Substituting S_R and S_T in (9) into (8) leads to the vector expression of radiation leave off reflector surface, i.e.,

$$\begin{bmatrix} R_{\mathrm{Qv}} \\ R_{\mathrm{Qh}} \\ R_{Q3} \\ R_{Q4} \end{bmatrix} = \begin{bmatrix} R_s + e_h(R_{\mathrm{rfl}} - R_s) + [(R_{\mathrm{rfl}} - R_s)(e_v - e_h)] \sin^2\theta \\ R_s + e_h(R_{\mathrm{rfl}} - R_s) + [(R_{\mathrm{rfl}} - R_s)(e_v - e_h)] \cos^2\theta \\ (R_{\mathrm{rfl}} - R_s) \cdot e_h \cdot (1 - e_h) \cdot \sin 2\theta \\ 0 \end{bmatrix}. \tag{10}$$

In the preceding equation, $e_h = 1 - r_h$ and $e_v = 1 - r_v$ are the reflector emissivities at H and V polarizations, respectively. $R_s = R_c$ when the reflector scans cold space, and $R_s = R_w$ when it scans to calibration blackbody target. Note that the QV/QH expressions derived here are actually consistent with those in (1), in which the model parameters β_0 and β_1 are expressed as functions of the emissivity and physical temperature of the reflector, i.e.,

$$\beta_0 = e_h(R_{\mathrm{rfl}} - R_s)$$
$$\beta_1 = (R_{\mathrm{rfl}} - R_s)(e_v - e_h).$$

Equation (10) provides a physical model for simulating pitch-over observations obtained through a scan antenna reflector. It can be seen that, when a nonlossless plane reflector is used to scan the scene, a uniform unpolarized radiation can be changed to polarized and expressed as a function of the antenna reflectivity, reflector physical temperature, scene temperature, and scan angle. Fig. 2 shows the simulated radiation in brightness temperature under different reflector temperatures and reflectivity conditions. For QV channels, it is a square of the sinusoidal curve, and for QH channels, it follows a cosine curve. It can be seen that the impact of reflector thermal radiation can become significant when the scene radiation is equal to the cosmic background, which is the case for cold space view in ATMS scan cycle. For example, if the reflector reflectivity is only 0.994, then the cold target brightness temperature being used in the calibration is no longer 2.73-K deep space brightness temperature; the thermal emission of the reflector with a magnitude as large as 4.5 K should be considered.

IV. Antenna Emission Estimated From Pitch-Over Observations

A. Antenna Emissivity Retrieval Model

In normal observations, ATMS continually scans the Earth scene, cold space, and warm load calibration target. During the pitch-over maneuver, the instrument turns to scan the unpolarized cold space instead of the Earth scene at each of 96 scan positions. Given that θ_s, θ_c, and θ_w are the scan angles for "Earth scene," cold space, and warm load, respectively, according to (10), the incident radiation from Earth scene is

$$R^s_{\mathrm{Qv}} = R_{\mathrm{rfl}} + r_h(R_c - R_{\mathrm{rfl}}) + \left[(R_c - R_{\mathrm{rfl}})\left(r_h^2 - r_h\right)\right] \sin^2\theta_s \tag{11a}$$
$$R^s_{\mathrm{Qh}} = R_{\mathrm{rfl}} + r_h(R_c - R_{\mathrm{rfl}}) + \left[(R_c - R_{\mathrm{rfl}})\left(r_h^2 - r_h\right)\right] \cos^2\theta_s. \tag{11b}$$

Similarly, for cold space and warm load views, we have

$$R^c_{\mathrm{Qv}} = R_{\mathrm{rfl}} + r_h(R_c - R_{\mathrm{rfl}}) + \left[(R_c - R_{\mathrm{rfl}})\left(r_h^2 - r_h\right)\right] \sin^2\theta_c \tag{11c}$$
$$R^c_{\mathrm{Qh}} = R_{\mathrm{rfl}} + r_h(R_c - R_{\mathrm{rfl}}) + \left[(R_c - R_{\mathrm{rfl}})\left(r_h^2 - r_h\right)\right] \cos^2\theta_c \tag{11d}$$
$$R^w_{\mathrm{Qv}} = R_{\mathrm{rfl}} + r_h(R_w - R_{\mathrm{rfl}}) + \left[(R_w - R_{\mathrm{rfl}})\left(r_h^2 - r_h\right)\right] \sin^2\theta_w \tag{11e}$$
$$R^w_{\mathrm{Qh}} = R_{\mathrm{rfl}} + r_h(R_w - R_{\mathrm{rfl}}) + \left[(R_w - R_{\mathrm{rfl}})\left(r_h^2 - r_h\right)\right] \cos^2\theta_w. \tag{11f}$$

Assume that C_s, C_c, and C_w are the corresponding receiver output counts for scene, cold space, and warm load, respectively, and $\delta = (C_s - C_c)/(C_w - C_c)$. By applying the two-point calibration equation for QV channels, we can derive

$$\frac{R^s_{\mathrm{QV}} - R^c_{\mathrm{QV}}}{R^w_{\mathrm{QV}} - R^c_{\mathrm{QV}}} = \delta. \tag{12}$$

Substituting (11) into (12), the antenna emissivity at 45° angle (w.r.t. the scattering plane) for ATMS QV channels can be solved as (13a), shown at the bottom of the next page.

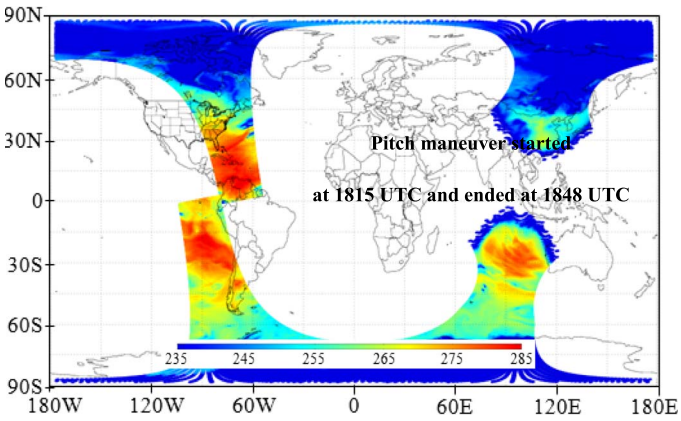

Fig. 3. SNPP ATMS orbital brightness temperatures at channel 18 on February 20, 2012.

Note that, for QH channels, following from (7), the antenna emissivity should be calculated as

$$\varepsilon_v = 1 - (1 - \varepsilon_h)^2. \tag{13b}$$

Since ε_v and ε_h are much less than 1, it follows that $\varepsilon_v = 2\varepsilon_h$.

By deriving (13), it is proved that the antenna emissivity can be accurately determined from space scan measurements by using the two-point calibration equation without considering receiver nonlinearity. Given the facts that the antenna emissivity is a small number, usually less than 0.01, to reach high accuracy of measurement, a well-known uniform scene with a temperature much lower than the physical temperature of the reflector is required, which can only be achieved through deep space scan.

B. Reflector Emissivity Spectrum

On February 18, 2012, the SNPP satellite was commanded to look over the cold space. For ATMS, this maneuver establishes a baseline radiometer output from pure cold space. As shown in Fig. 3, the maneuver started at 1815 UTC and ended at 1848 UTC, and thus, a large portion of this 33-min period is over oceans. The spacecraft is pitched completely off the Earth to enable all the instruments to acquire full scans of deep space, permitting the deviations from the uniformity of the field of view to be characterized. When the Earth's disk lies totally outside the scan direction, there should be good sensitivity for the all the instruments to see any anomalies introduced by obstacles near the spacecraft itself and radiation emitted from the ATMS scanning system and the other instruments. For SNPP mission, Earth is visible by ATMS antenna at 62.37° (local zenith angle of 27.63°) from nadir, assuming that the Earth diameter is approximated 6100 km. Since the ATMS cross-scan swath is about 2600 km, complete ocean views are possible if the maneuver is performed over the Indian, S. Atlantic, N. Atlantic, and Pacific Ocean regions [13].

Fig. 4 shows ATMS antenna brightness temperatures at channels 1 and 3 from all the data processed by the joint polar satellite system (JPSS) ground software, which is called Algorithm Dynamic Library (ADL) version 5.11, in which a full radiance calibration is applied. Note that the data point

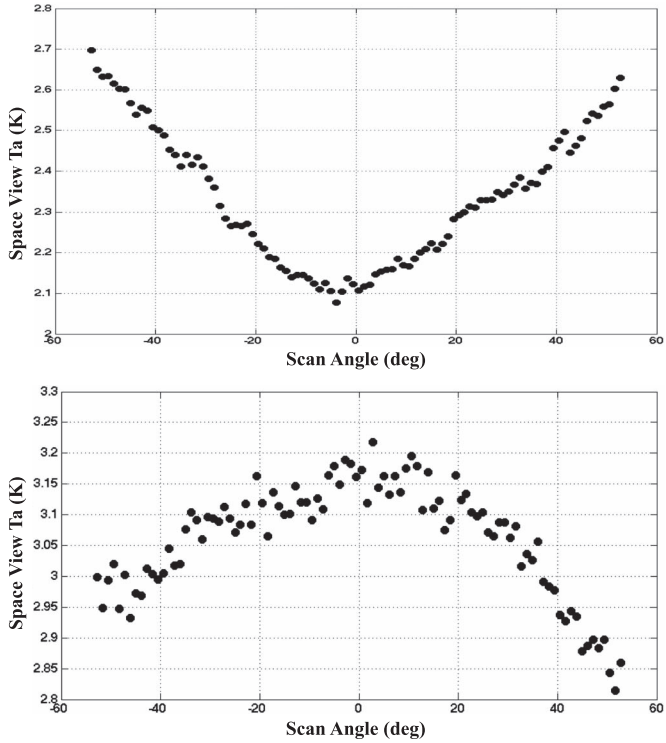

Fig. 4. Examples of SNPP ATMS mean brightness temperature versus scan angle for (upper panel) channels 1 and (lower panel) 3 derived from the pitch maneuver observations.

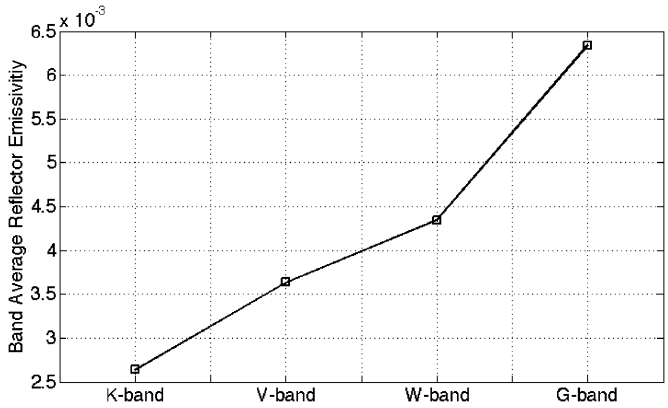

Fig. 5. Retrieved antenna reflector emissivity for ATMS. H-pol for K-/W-bands and V-pol for V-/G-bands.

at each scan position is averaged from all the observations between 1820 UTC and 1845 UTC when ATMS scans through space. It is shown that the bias at each channel depends on the scan angle. The patterns for QV polarization at channels 1, 2, and 16 have a "smile" shape, whereas those for QH polarization have a "frown" shape. The bias at the nadir positions and the scan-angle-dependent bias can be well explained by the antenna emission model established in the previous section.

Based on the pitch-over observation data sets described earlier, the ATMS reflector emissivity is determined by using the model expressed in (13) and is shown in Fig. 5. It should be noted that, since the reflector emissivity is defined w.r.t. the reflector scanning plane, which is different from the Earth surface scattering plane in which the instrument polarization is defined, the retrieved H-pol emissivity should be used for

TABLE II
RETRIEVED ANTENNA REFLECTOR EMISSIVITY AT V-POL (K-/W-BANDS) AND H-POL (V-/G-BANDS)

Bands Name	Reflector Emissivity
K	0.0026
V	0.0036
W	0.0043
G	0.0063

QV channels and the V-pol emissivity for QH channels. The retrieved emissivity at each band is listed in Table II. In general, the spectral emissivity is in a range of 0.0026 to 0.0063. The emissivity at V-polarization is larger than that at H-polarization (figure is omitted). Compared with the emissivity computed from Skou's equation, the retrieved ATMS emissivity is much larger, with a factor of 6 higher for 23.8 GHz and 5 higher for 183 GHz. Since the reflector emission cannot be ignored, it needs to be evaluated and corrected in calibration process.

C. Impact of Antenna Emissivity on the Earth Observations

For NWP applications, an ATMS calibration error of less than 1 K (0.75 K for V-band) is required [14]. Therefore, it is important for users to know the impact of antenna emissivity on the accuracy of data products. Since the radiation from cold space, warm load, and Earth scene are all collected through the polarized flat reflector, the impact of antenna emissivity on Earth scene includes two parts: extra error will be introduced into the calibration equation due to uncorrected antenna emissivity on calibration target, and the calibrated Earth scene brightness temperature will be contaminated directly by the reflector thermal radiation if not corrected. In this paper, we mainly focused on assessing the impact of antenna emissivity on calibration accuracy. Its impact on observed Earth scene brightness temperature will be discussed in future work.

To evaluate the impact of antenna emissivity on calibration accuracy, we need to start from the calibration equation of the ATMS instrument, i.e.,

$$R_s = R_{bI} + Q_b. \tag{14}$$

In the preceding equation, R_{bI} is the linear part of the calibrated scene temperature and can be computed from calibration targets by the two-point calibration equation as

$$R_{bI} = \delta \cdot (R_w - R_c) + R_c \tag{15}$$

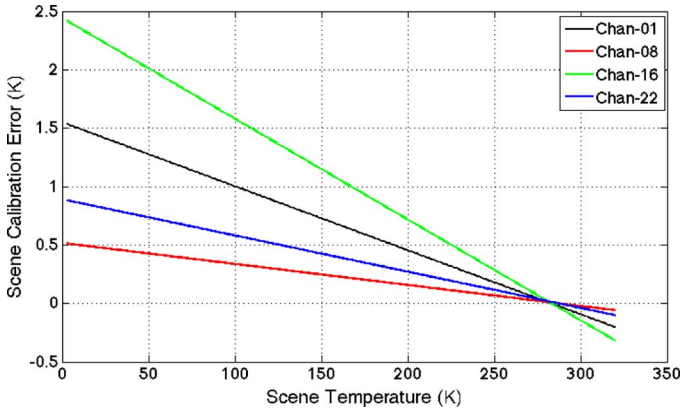

Fig. 6. Scene-temperature-dependent calibration error at the K-, V-, W-, and G-bands of ATMS from error model. The temperatures of reflector and warm load are retrieved from on-orbit PRT measurements of ATMS; nonlinearity parameters are derived from SNPP ATMS TVAC test under middle receiver temperature conditions.

where R_w and R_c are the radiance for warm load and 2.7-K cold space, respectively; and $\delta = (C_s - C_c)/(C_w - C_c)$.

In (14), Q_b is the nonlinear part of the calibrated scene temperature, which can be expressed as a function of the maximum nonlinearity $Q_{\max}$ as follows:

$$\begin{aligned} Q_b &= Q_{\max} \cdot \left[4 \cdot (\delta - 0.5)^2 - 1\right] \\ Q_{\max} &= \frac{1}{4} \cdot \mu \cdot (R_w - R_c)^2 \end{aligned} \tag{16}$$

where μ is the nonlinearity parameter and can be derived from thermal vacuum (TVAC) test data.

The error model for calibrated scene temperature due to antenna emissivity correction can be built from (14)–(16) as

$$\begin{aligned} \Delta R_s = \delta \cdot (\Delta R_w - \Delta R_c) + \Delta R_c + \frac{1}{4} \cdot \Delta\mu \cdot (\Delta R_w - \Delta R_c)^2 \\ \cdot [4 \cdot (\delta - 0.5)^2 - 1]. \end{aligned} \tag{17}$$

It can be seen from (17) that the calibration errors arising from antenna emission depend on three terms: radiance error in cold space and warm load and error in nonlinearity parameters. From (11), an explicit form of radiance error in calibration target can be derived as follows.

For QV channels

$$\Delta Rx = \varepsilon_h (R_{\text{rfl}} - R_x) + (R_{\text{rfl}} - R_x) \cdot (\varepsilon_v - \varepsilon_h) \cdot \sin^2 \theta_x. \tag{18a}$$

For QH channels

$$\Delta Rx = \varepsilon_h (R_{\text{rfl}} - R_x) + (R_{\text{rfl}} - R_x) \cdot (\varepsilon_v - \varepsilon_h) \cdot \cos^2 \theta_x. \tag{18b}$$

In (18), ΔRx can be ΔR_c or ΔR_w.

$$\varepsilon_h = \frac{\delta (R_w - R_c)}{\delta \left[(R_w - R_{\text{rfl}}) \sin^2 \theta_w - (R_c - R_{\text{rfl}}) \sin^2 \theta_c\right] - (R_c - R_{\text{rfl}})(\sin^2 \theta_s - \sin^2 \theta_c)}. \tag{13a}$$

By using (17), the impact of antenna emissivity to calibration error can be then assessed. Fig. 6 shows the scene-temperature-dependent calibration error at the K-, V-, W-, and G-bands of ATMS. To derive the simulation results, the temperatures of reflector and warm load are retrieved from on-orbit platinum resistance thermometers (PRT) measurements of ATMS; nonlinearity parameters are derived from SNPP ATMS TVAC test under middle receiver temperature conditions.

It can be seen that the calibration error decreases with increased scene temperature. For K-band, the calibration error can be as large as 1.5 K at 2.7-K space view, and decreases to -0.1 K at 300-K Earth scene observation. Due to the different reflectivity characteristics at ATMS channels, the magnitude of calibration error at different channels is also different. W-band was observed to have the largest error, which can be explained by the relatively larger emissivity in this channel, coupled with the QV polarization, which produces the largest error at a 90° view angle, close to that of the space view.

V. Conclusion and Discussion

The ATMS antenna reflector can emit the radiation due to the coating material and surface roughness and have an impact on calibration accuracy. Its cross-track rotation can complicate its emission problem by changing the polarization state of incident wave. When reflector reflectivity approaches 1, it is very difficult to be measured in ground test. Since no improvements have been made for the JPSS-1 ATMS antenna, pitch-over maneuver operation is very critical for the measurement of the reflector emissivity spectrum in space; it provides a very unique data set from which the reflector emissivity can be retrieved from the deep space observations with very high accuracy, which is not achievable in ground test. In this paper, we have developed a technique to estimate the ATMS plane reflector emission for frequency ranging from K- to W-bands. Using the Mueller matrix of reflection and transmission at 45° angle for a bulk-material reflector, we derived a full vector expression for reflected radiation for a nonlossless rotating reflector. The physical model is then applied to the two-point calibration equation, and the antenna emissivity can be derived from the pitch-over observations. The reflector emissivity spectrum ranges from 0.002 to 0.006 from K- to G-bands.

An error model is also developed to assess the impacts of antenna emissivity to calibration. Results show that the calibration error can be as large as 2.5 K for space view at channel 16. The error is scene dependent and is different for different channels of ATMS due to the frequency dependence of the reflector emissivity and the different channel polarizations. To compute the error in the ATMS TDRs, it is necessary to take account of both the calibration error presented in this paper and of the influence of the reflector emission when Earth is viewed. For unpolarized channels, the scan-dependent feature of TDR error is dominated by sine-square term at QV channels and cosine-square term in QH channels. For polarized window channels, the impacts of antenna emissivity to observed scene brightness temperature are complicated by the rotation of polarization state, which will be studied in our future work.

References

[1] F. Weng, X. Zou, X. Wang, S. Yang, and M. D. Goldberg, "Introduction to Suomi National Polar-orbiting Partnership Advanced Technology Microwave Sounder for numerical weather prediction and tropical cyclone applications," *J. Geophys. Res.*, vol. 117, 2012, Art. no. D19112, doi: 10.1029/2012JD018144.

[2] F. Weng, H. Yang, and X. Zou, "On convertibility from antenna to sensor brightness temperature for ATMS," *IEEE Geosci. Remote Sens. Lett.*, vol. 10, no. 4, pp. 771–775, Jul. 2013.

[3] R. W. Saunders, T. J. Hewison, S. J. Stringer, and N. C. Atkinson, "The radiometric characterization of AMSU-B," *IEEE Trans. Microw. Theory Techn.*, vol. 43, no. 4, pp. 760–771, Apr. 1995.

[4] T. Labrot, L. Lavanant, K. Whyte, N. Atkinson, and P. Brunel, "AAPP documentation: Scientific description," NWP SAF Doc., Darmstadt, Germany, NWPSAF-MF-UD-001, v7.0, 2011. [Online]. Available: http://www.nwpsaf.eu/deliverables/aapp/index.html

[5] T. J. Kleespies *et al.*, "Evaluation of scan asymmetry in the NOAA-14 microwave sounding unit by a pitch maneuver," *IEEE Geosci. Remote Sens. Lett.*, vol. 4, no. 4, pp. 621–623, Oct. 2007.

[6] T. J. Kleespies, "Recharacterization of the Microwave Sounding Unit cross-track asymmetry during a spacecraft tumble," *IEEE Trans. Geosci. Remote Sens. Lett.*, vol. 8, no. 2, pp. 230–232, Mar. 2011.

[7] B. Yan and F. Weng, "Assessments of F16 special sensor microwave imager and sounder antenna temperatures at lower atmospheric sounding channels," *Adv. Meteorol.*, vol. 2009, 2009, Art. no. 420985, doi: 10.1155/2009/420985.

[8] B. Kunkee, S. D. Swadley, G. A. Poe, Y. Hong, and M. F. Werner, "Special Sensor Microwave Imager Sounder (SSMIS) radiometric calibration anomalies—Part I: Identification and characterization," *IEEE Trans. Geosci. Remote Sens.*, vol. 46, no. 4, pp. 1017–1033, Apr. 2008.

[9] W. Bell *et al.*, "An initial evaluation of SSMIS radiances for radiance assimilation applications," in *Proc. IEEE MicroRad*, 2006, pp. 207–211.

[10] N. Skou, "Measurement of small antenna reflector losses for radiometer calibration budget," *IEEE Trans. Geosci. Remote Sens.*, vol. 35, no. 4, pp. 967–971, Jul. 1997.

[11] D. Goldstein, *Polarized Light*, 2nd ed. New York, NY, USA: Marcel Dekker, 2013.

[12] A. Ishimaru, *Electromagnetic Wave Propagation, Radiation, and Scattering*. Englewood Cliffs, NJ, USA: Prentice-Hall, 1991.

[13] F. Weng *et al.*, "Calibration of Suomi National Polar-orbiting Partnership (NPP) Advanced Technology Microwave Sounder (ATMS)," *J. Geophys. Res.*, vol. 118, no. 19, pp. 11 187–11 200, Oct. 2013.

[14] E. Kim, C.-H. J. Lyu, K. Anderson, R. V. Leslie, and W. J. Blackwell, "S-NPP ATMS instrument prelaunch and on-orbit performance evaluation," *J. Geophys. Res. Atmos.*, vol. 119, no. 9, pp. 5653–5670, May 2014, doi: 10.1002/2013JD020483.

Hu Yang (M'09) received the Ph.D. degree from the Chinese Academy of Sciences, Beijing, China, in 2003.

During 2003–2011, he was a Senior Research Scientist with the National Satellite Meteorological Center, China Meteorological Administration, leading the microwave instrument calibration and satellite ground application system development as the Instrument Scientist and the Program Scientist. In 2012, he joined the Earth System Science Interdisciplinary Center, University of Maryland, College Park, MD, USA, working on Suomi National Polar-orbiting Partnership (NPP)/JPSS Advanced Technology Microwave Sounder calibration/validation as a Project Principal Investigator. He has authored or coauthored over 40 peer-reviewed journals. His main study field includes passive microwave radiometer calibration/validation, satellite geolocation, and satellite observation simulation.

Dr. Yang was a recipient of the 2010 National Defense Science Advancement Award from the China Aeronautic and Space Agency for his outstanding contribution to the development of China's first spaceborne microwave imager radiometer.

Fuzhong Weng received the Ph.D. degree from Colorado State University, Fort Collins, CO, USA, in 1992.

He is currently the Chief of Satellite Meteorology and Climatology of NOAA/NESDIS/Center for Satellite Applications and Research, a Senior Scientist of the Joint Center for Satellite Data Assimilation, and a JPSS Sensor Science Chair. He has authored or coauthored over 150 papers in American journals (e.g., American Meteorological Society, American Geophysical Union, and IEEE) and other international journals.

Dr. Weng was a recipient of a number of awards, including the first winner of the 2000 NOAA David Johnson Award for his outstanding contributions to satellite microwave remote sensing fields and the utilization of satellite data in the NWP models, the U.S. Department of Commerce Gold Medal Award in 2005 for his achievement in satellite data assimilation, the NOAA bronze medal for leading successful NOAA-18 instrument calibration, and the NOAA Administrator's Award for developing new and powerful radiative transfer models to assimilate advanced satellite data.

Kent Anderson received the B.S. and M.S. degrees in electrical engineering from the Rose-Hulman Institute of Technology, Terre Haute, IN, USA, in 1971 and 1972, respectively.

He has 30 years of experience in systems engineering for spaceborne remote sensing systems. For the last 15 years, he has been the Lead Systems Engineer for Civil Space Programs with the Northrop Grumman Electronic Systems, Linthicum Heights, MD, USA, where he is focused primarily on millimeter-wave radiometry, particularly for the Advanced Technology Microwave Sounder Program. His primary contributions have been in requirements management, initial design trade studies, performance analyses, and analyses of test data.